Faraday Discussions

Synthesis of Metallic Mixed 3R and 2H $Nb_{1+x}S_2$ Nanoflakes by Chemical Vapor Deposition

Journal:	*Faraday Discussions*
Manuscript ID	FD-ART-12-2019-000132.R1
Article Type:	Paper
Date Submitted by the Author:	19-Jan-2020
Complete List of Authors:	Mohmad, Abdul Rahman; National University of Malaysia, Hamzah, Azrul Azlan; Univ Kebangsaan Malaysia Yang, Jieun; University of Cambridge Wang, Yan; University of Cambridge Bozkurt, Ibrahim; Rutgers The State University of New Jersey, Materials Science and Engineering Shin, Hyeon Suk; Ulsan National Institute of Science and Technology, Interdisciplinary School of Green Energy Jeong, Hu Young; UNIST, UNIST Central Research Facilites Chhowalla, Manish; University of Cambridge

ARTICLE

Synthesis of Metallic Mixed 3R and 2H $Nb_{1+x}S_2$ Nanoflakes by Chemical Vapor Deposition

Received 00th January 20xx,
Accepted 00th January 20xx

DOI: 10.1039/x0xx00000x

Abdul Rahman Mohmad,*[a] Azrul Azlan Hamzah,[a] Jieun Yang,[b] Yan Wang,[b] Ibrahim Bozkurt,[c] Hyeon Suk Shin,[d] Hu Young Jeong [e] and Manish Chhowalla *[b]

In this work, we report the synthesis and characterization of mixed phase $Nb_{1+x}S_2$ nanoflakes prepared by chemical vapor deposition. The as-grown samples show high density of flakes (thickness ~50 nm) that form a continuous film. Raman and X-ray diffraction data show that the samples consist of both 2H and 3R phases with the 2H phase containing high concentration of Nb interstitials. These Nb interstitials sit in between the NbS_2 layers to form $Nb_{1+x}S_2$. The cross-sectional Electron Dispersive Spectroscopy analysis in transmission electron microscope suggests that the 2H $Nb_{1+x}S_2$ region is found in thinner flakes while the 3R NbS_2 is observed in thicker regions of the films. The evolution of the phase from 2H $Nb_{1+x}S_2$ to 3R NbS_2 may be attributed to the change of growth environment from Nb rich at the start of the growth to sulfur rich at the latter stage. It was also found that the incorporation of Nb interstitials is highly dependent on the temperature of $NbCl_5$ precursor and the position of the substrate in the furnace. Samples grown at high $NbCl_5$ temperature and substrate located closer to the $NbCl_5$ source show higher incorporation of Nb interstitials. Electrical measurements show linear I-V characteristics indicating metallic nature of the $Nb_{1+x}S_2$ film with relatively low resistivity of 4.1×10^{-3} Ωcm.

Introduction

The use of hydrogen as energy carrier could address the issues of sustainability, energy security and environmental emissions. Hydrogen is also a key agent in many industrial processes including refining industries, chemical industries and electronic sector. The generation of hydrogen via electrochemical reduction of protons requires a catalyst that is typically expensive platinum. Electrocatalysts based on layered or 2-dimensional transition metal dichalcogenides (TMDs) have attracted significant interest due to its low cost and high intrinsic activity per unit site.[1-5]

Based on the theoretical work reported by Tsai *et al.,* the basal planes of metallic TMDs (eg. 1T MoS_2, 2H NbS_2 and 2H VS_2) are the most active with hydrogen adsorption free energy, ΔG_H, close to thermo-neutral (~0.04–0.3eV).[6] The most widely studied metallic TMD is 1T MoS_2 and this material has been shown to have excellent hydrogen evolution reaction (HER) properties.[7, 8] However, MoS_2 is typically found in semiconducting 2H phase and phase transformation via lithium intercalation is required to transform the 2H to 1T phase. This process is not straightforward, involves highly flammable chemical and yield concentration of 1T phase of ~50-80%.[7, 9, 10] The phase transformed 1T MoS_2 is metastable that relaxes to its original 2H phase when exposed to high temperatures.[10]

Another promising catalyst for HER is metallic NbS_2 but this material has not been extensively studied compared to 1T MoS_2. This is mainly due to challenges in synthesizing high quality and thin NbS_2 nanoflakes. Most previous works have reported 3R NbS_2 with relatively thick flakes on SiO_2 (thickness 20-400 nm).[11, 12] Monolayer and multilayers NbS_2 have been reported on hBN substrate.[13, 14] The chemical vapor deposition (CVD) conditions used to synthesize NbS_2 vary significantly between reports.[11-13, 15, 16] For example, NbS_2 reported by Ge *et al.* was grown for 10 minutes while the growth duration used by Yanase *et al.* was between 30-120 minutes.[11, 12] For carrier gas, Ge *et al.* used 200 sccm of Argon but Yanase *et al.* used significantly higher ArH_2 flow rate of 800-2000 sccm.[11, 12] The large variations in CVD conditions between reports suggest that the growth of NbS_2 on SiO_2 is not well understood and require further investigation. In this work, we report the synthesis of mixed phase $Nb_{1+x}S_2$. The effect of growth conditions on the incorporation of Nb interstitials between NbS_2 layers will be discussed. Finally, evidence of mixed 2H and 3R phases in our samples will be presented.

[a] Institute of Microengineering and Nanoelectronics, National University of Malaysia, 43600 UKM Bangi, Malaysia. Email: armohmad@ukm.edu.my
[b] Department of Materials Science and Metallurgy, University of Cambridge, 27 Charles Babbage Road, Cambridge CB3 0FS, UK. Email:mc209@cam.ac.uk
[c] Materials Science and Engineering, Rutgers University, 607 Taylor Road, Piscataway, New Jersey 08854, USA.
[d] Dept. of Chemistry and Dept. of Energy Engineering, Low-Dimensional Carbon Materials Center, Ulsan National Institute of Science and Technology (UNIST), UNIST-gil 50,Ulsan 44919, Republic of Korea.
[e] UNIST Central Research Facilities (UCRF) and School of Materials Science and Engineering, UNIST, Ulsan 689-798, Republic of Korea
†Electronic Supplementary Information (ESI) available: Furnace temperature profile and AFM images. See DOI: 10.1039/x0xx00000x

Experimental

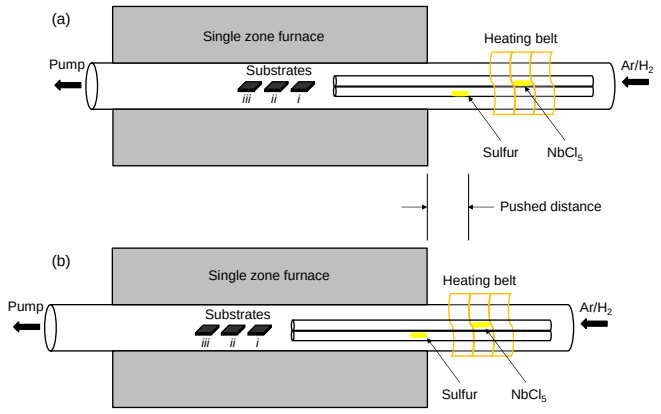

Fig. 1 Schematic of the CVD setup during (a) temperature ramping-up and (b) growth. The precursors were kept separate using smaller diameter tubes. A heating belt was used to vaporize $NbCl_5$ while sulfur was sublimated by moving to edge of the zone furnace during growth.

The $Nb_{1+x}S_2$ samples reported in this work were grown by thermal CVD in a single tube furnace with a diameter of 2.5 cm at 20 Torr pressure using niobium chloride ($NbCl_5$, Alfa Aesar, 99.9%) and sulfur as the precursors (Alfa Aesar, 99.5%). The $NbCl_5$ powder (40-60 mg) was located upstream followed by sulfur (200-400 mg) and the substrate (300 nm SiO_2 on Si), as shown in Fig. 1. The temperature of the $NbCl_5$ source was independently controlled by a heating belt while the sulfur was positioned at the edge of the single zone furnace. Both of the precursors were located in two separate tubes with diameters of 1 cm within the larger 2.5 cm tube to prevent cross contamination.

The growth tube was initially evacuated at 20 Torr for 30 minutes. Then, the temperature of the furnace was increased from room temperature to 1000 °C in 40 minutes followed by heating the belt to ~260-320 °C in 5 minutes. As soon as the temperature of the belt reached 200 °C, the tube containing $NbCl_5$ was pushed to the growth position. At this point, the edge of the furnace is sufficiently hot to sublimate the sulfur. The growth was carried out at 1000 °C for ~12 minutes. The carrier gas was Ar/H_2 (H_2 10%) with a flow rate of 80 sccm was introduced throughout the growth process. Once the growth finished, the furnace and heating belt was cooled down naturally to room temperature. The furnace temperature profile versus time is shown in Fig. S1.

The as-grown samples were analysed using scanning electron microscopy (Zeiss Sigma Field Emission SEM) and X-ray diffraction (PANAnalytical PW3040/60) with Cu-K_α radiation (λ=1.5418 Å). Renishaw InVia Raman with excitation wavelength of 514 nm and laser spot size of 1 μm was used to measure the vibrational spectra. For the cross-sectional Transmission Electron Microscope (TEM) imaging, the sample was prepared by Focused Ion Beam and Energy Dispersive Spectroscopy was measured using JEOL microscope (JEM-2100F). For electrical characterization, $Nb_{1+x}S_2$ devices were fabricated by using a shadow mask and evaporating 100 nm of Au contact to create devices with channel lengths between 20 to 100 μm. The current-voltage measurements were carried out using Keithley 4200A-SCS Parameter Analyzer.

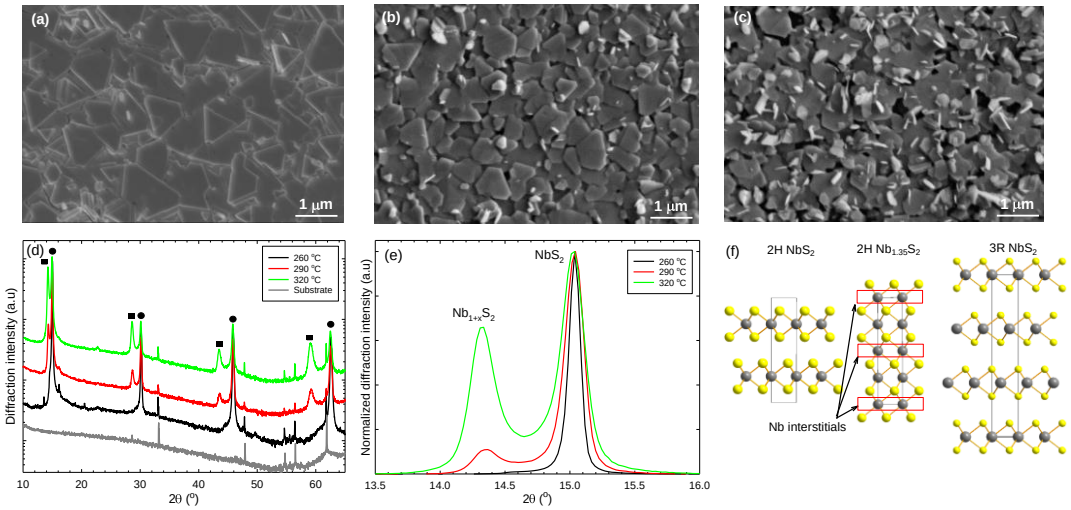

Fig. 2 SEM images of NbS_2 samples grown with different $NbCl_5$ precursor temperatures. The $NbCl_5$ temperatures that were investigated are: (a) 260 °C, (b) 290 °C and (c) 320 °C. (d) XRD spectra of SiO_2/Si substrate and NbS_2 samples shown in (a)-(c). The peaks labelled with solid circles and squares are diffraction peaks from NbS_2 and 2H $Nb_{1+x}S_2$, respectively. (e) Close up XRD spectra near the (002) diffraction peak. The intensity is normalized to the intensity of the NbS_2 peak. (f) Atomic arrangements in 2H NbS_2, 2H $Nb_{1+x}S_2$ and 3R NbS_2.

ARTICLE

Results and discussion

Fig. 2(a)-(c) shows scanning electron microscope (SEM) images of NbS_2 samples grown at different $NbCl_5$ temperatures, T_{NbCl5} of 260 °C, 290 °C and 320 °C. The sample grown at T_{NbCl5} = 260 °C shows high density of triangular flakes that form a continuous film. The individual flake is horizontally oriented with lateral dimension of ~1 µm. However, for samples grown at higher T_{NbCl5} = 290 and 320 °C, horizontal as well as vertical flakes were observed. The vertical flakes sit on top of horizontal flakes and their density increases with an increase in T_{NbCl5}. This observation suggests that growth initially starts with the formation of nucleation sites followed by layer-by-layer growth to form 2D islands. The 2D islands will then coalesce to form a complete layer. However, rapid merge or collision between the 2D islands under high concentration of reactants may cause the growth plane to curl, resulting in the formation of NbS_2 seedlings.[17] Hence, higher density of NbS_2 seedlings or vertical flakes are observed with the increase of T_{NbCl5}.

X-ray diffraction (XRD) measurements were carried out to investigate the structural properties of as-grown flakes, as shown in Fig. 2 (d). All samples show diffraction peaks at 15, 30.2, 45.9 and 62.6°. These peaks fit nicely with the (00*l*) diffraction peaks of 2H (JSPDS#97-004-3697) and 3R NbS_2 (JSPDS#97-004-3696). Since the positions of the diffraction peaks are very close for both phases, it is difficult to differentiate between the two phases based on these diffraction peaks alone. Samples grown at T_{NbCl5} = 290 and 320 °C show additional peaks at 14.4, 28.7, 43.6 and 59.2°. These peaks may be attributed to the (00*l*) diffraction peaks of non-stoichiometric $Nb_{1+x}S_2$ due to the incorporation of Nb interstitials between the NbS_2 layers. [12, 18-21] The excess Nb will cause the lattice to expand in the *c*-axis direction which results in diffractions at smaller angles compared to the stoichiometric NbS_2. [12,20,26] Based on the 0.6° of peak separation between the $Nb_{1+x}S_2$ and NbS_2, it is estimated that x is ~0.3. Our data is also consistent with the diffraction pattern coming from the (00*l*) planes of 2H $Nb_{1.35}S_2$ (JSPDS#97-004-3699). It was proposed that the Nb atoms within the NbS_2 layers are located in trigonal prismatic coordination while the Nb interstitials that sit between the NbS_2 layers are located in octahedral sites [Fig. 2 (f)]. [20] The intensity of the $Nb_{1.3}S_2$ peak also increases with the increase of T_{NbCl5} as shown in Fig. 2 (e). The peak intensity ratio of $Nb_{1.3}S_2/NbS_2$ is ~0, 0.11 and 0.66 for T_{NbCl5} of 260, 290 and 320 °C, respectively. These results indicate higher incorporation of Nb interstitials with increasing T_{NbCl5}, as expected.

The effects of substrate position on the morphology of NbS_2 nanoflakes were also investigated, as shown in Fig. 3. For this study, T_{NbCl5} was fixed at 320 °C and substrates were placed at three different positions labelled as *i*, *ii* and *iii*. Position *i* is located at the center of the furnace and positions *ii* and *iii* are located downstream with a separation distance of 1 cm (Fig. 1). The temperature difference between position *i* and *iii* is ~10 °C. Based on the SEM images, the overall density of NbS_2 flakes reduces and the density of vertical and slanted flakes increases as the substrate is located away from the center of the furnace. It is also important to note that for sample at position *i*, the vertical flakes grew on top of horizontal flakes while for sample *iii*, the vertical and slanted flakes grew directly on the substrate. These observations may be explained by the reduction of precursor concentration and lower substrate temperature as the substrate is located downstream and away from the center of the furnace.

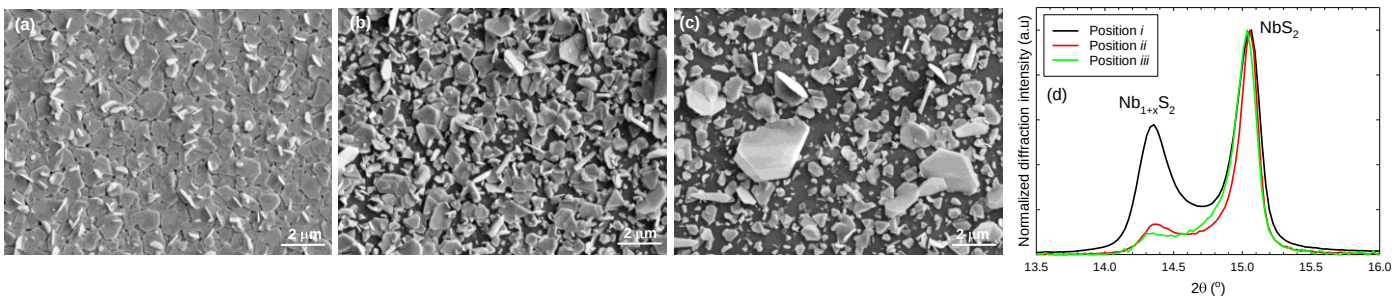

Fig. 3 Morphology of NbS_2 samples grown at substrate position (a) *i*, (b) *ii* and (c) *iii*. Position *i* is located at the center of the furnace followed by position *ii* and *iii* towards downstream. (d) Close up XRD spectra near (002) diffraction peak for samples in (a)-(c).

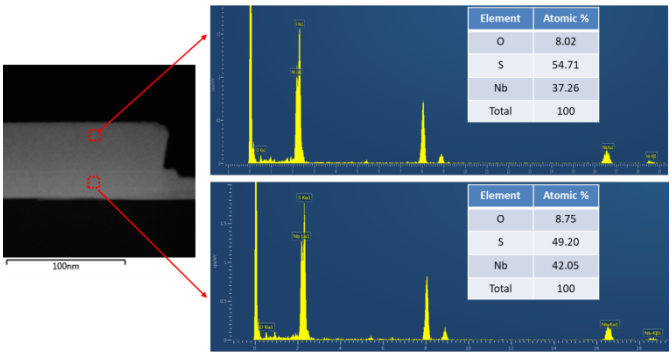

Fig. 4 Cross-sectional TEM image and EDS measured at the top and bottom of the film as indicated by the red squares.

For sample at position *i*, vertical NbS_2 flakes formed on top of 2D islands due to high substrate temperature and high concentration of reactants, similar to observations in Fig. 2. However, for sample at positions *ii* and *iii*, the reduction of precursor concentration resulted in lower nucleation sites and lower density of flakes. The growth of vertical flakes directly on the substrate can be explained by the Volmer-Weber growth mechanism in which surface diffusion of adatoms is limited at low growth temperature. Our observations are consistent with other reports that also obtained vertical NbS_2 and SnS_2 flakes directly on substrates at lower growth temperatures (300–800 °C). [11, 14, 22, 23]

Fig. 3 (d) shows the corresponding XRD spectra of the samples grown at positions *i* to *iii*. All samples show two main peaks at 14.4° and 15° that are similar to the results shown in Fig. 2 (e). Based on the ratio between $Nb_{1+x}S_2$ and NbS_2, sample at position *i* has the highest concentration of Nb interstitials followed by position *ii* and *iii* samples. The results indicate that substrates located closer to the $NbCl_5$ source are exposed to higher concentration of Nb vapor which results in higher incorporation of Nb interstitials. This highlights the importance of substrate position as it can significantly affect the morphology and concentration of Nb interstitials in the samples.

To further understand the incorporation of Nb interstitials in our sample, cross-sectional TEM with Energy Dispersive Spectroscopy (EDS) analyses was carried out. The TEM image in Fig. 4 shows that the thickness of the $Nb_{1.3}S_2$ nanoflake is ~50 nm. The Energy Dispersive Spectroscopy (EDS) analysis was carried out to detect niobium, sulfur and oxygen at two different regions; (i) thin film region at the bottom of the flake and (ii) thick film region at the top of the flake. It was found that higher Nb signal (with respect to sulfur) was detected at the bottom of the flake compared to the top region. This suggests that the concentration of Nb interstitials is not homogeneous across the sample with the bottom area showing higher incorporation of Nb interstitials compared to the top. A small percentage of oxygen (8-9%) was also detected. Since the concentration of oxygen is almost similar in both regions, it suggests that oxidation may have happened during growth (not after the growth) due to partially oxidized $NbCl_5$ precursor. It is well known that $NbCl_5$ is sensitive to moisture in air and oxidation may happen during the transfer of the powder from the glove box into the growth tube.

In order to identify the phase of the NbS_2 flakes, Raman spectroscopy measurements were carried out, as shown in Fig. 5. We found that all samples show three main peaks at 330, 387 and 407 cm^{-1}, which are the features of E_2, A_1 and A_2 vibration modes of the 3R NbS_2, respectively.[11, 12, 15, 24] Additional peaks were also observed at 228 (position *i* sample only) and 365 cm^{-1} and a shoulder at ~306 cm^{-1}. These additional peaks are close to the calculated frequencies of the E_{1g}, A_{1g} and E^1_{1g} modes of 2H NbS_2 that are at 227, 363 and 296 cm^{-1}, respectively.[25] The results are interesting as it suggests that both phases are present in the samples. To the best of our knowledge, this is the first time mixed 2H and 3R phase NbS_2 have been synthesized by CVD. One possible explanation is due to the phase limit of the non-stoichiometric $Nb_{1+x}S_2$. According to Jellinek *et al*, the phase limit at 1000 °C for 3R $Nb_{1+x}S_2$ is between $0.12<x<0.25$ while the phase limit for 2H $Nb_{1+x}S_2$ is between $0.3<x<0.43$.[20] Even though Kadijk *et al* and Hodouin reported slightly different values of phase limit, their findings are similar in which the concentration limit of Nb interstitials is higher in 2H phase compared to 3R.[18, 21] Based on these reports and x ~ 0.3 in our sample, it is very likely that the thin regions of the flake is 2H $Nb_{1.3}S_2$ while the top region is 3R due to high concentration of Nb at the bottom compared to the top (Fig. 4). This is also consistent with our detailed STEM analysis reported by Yang *et al*.[26]

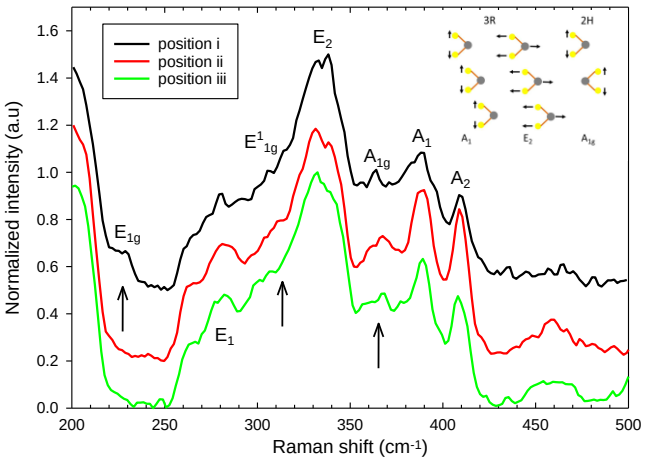

Fig. 5 Raman spectra of NbS_2 samples grown at different substrate positions. The black arrows indicate Raman modes for 2H phase NbS_2. Schematic of the vibrational modes for the two phases are shown in the inset.

It is also important to discuss why Nb incorporation changes with thickness. We believe that this phenomenon may be related to the growth procedure. When the temperature of the furnace is at 1000 °C and T_{NbCl5} reaches 200 °C, the tube containing sulfur was pushed to the growth position to start sublimation and the growth process. It is possible that the pushing technique introduced a delay in the supply of sulfur vapor which creates a temporary period of Nb rich environment. This results in the initial growth of 2H $Nb_{1.3}S_2$ with high concentration of Nb interstitials. As sulfur vapor increases with time, the growth environment changes from Nb rich to sulfur rich. Hence, concentration of the Nb interstitials reduces and the growth is shifted to 3R phase. This could explain the formation of 3R phase NbS_2 on top of the 2H $Nb_{1.3}S_2$. By controlling the growth duration, one may also obtain thin flakes (<20 nm) that are purely 2H $Nb_{1+x}S_2$ and thick flakes that are mixed phase but dominated by the 3R.

Mixed phase $Nb_{1.3}S_2$ electronic devices with channel lengths between 20 to 100 µm were fabricated and the typical I-V curve is shown in Fig. 6. The I-V measurements were carried out between -2 to 2 V with current compliance of 10 mA. The thickness of the $Nb_{1.3}S_2$ film is ~50 nm and the AFM image of the film is shown in Fig. S2. The I-V data show that the device has a linear I-V characteristic which indicates ohmic contact with metallic $Nb_{1.3}S_2$ channel. At 0.5 V, the measured current is as high as 9.8 mA which correspond to current density of 2.5×10^4 Acm^{-2}. Based on measurements on 13 such devices, the average resistivity of the $Nb_{1.3}S_2$ films was found to be 4.1×10^{-3} Ωcm. This value is approximately two orders of magnitude lower than the resistivity of the more established metallic 1T MoS_2.[7] The significantly lower resistivity is expected to increase carrier injection efficiency making $Nb_{1+x}S_2$ as a promising candidate for HER.

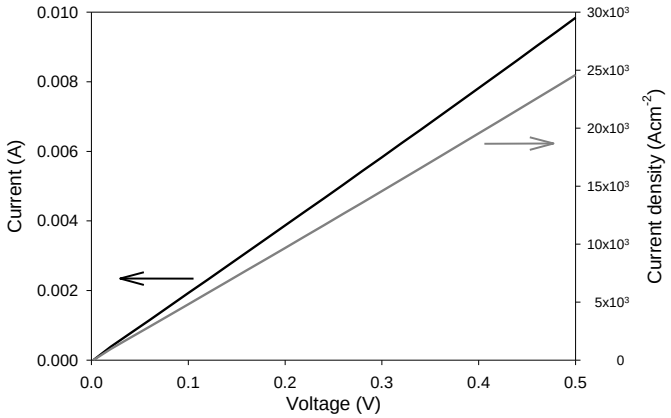

Fig. 6 Current-voltage characteristics of the fabricated $Nb_{1+x}S_2$ device. The solid black and grey refer to current and current density, respectively.

Conclusions

In summary, we have studied mixed phase and non-stoichiometric $Nb_{1+x}S_2$ nanoflakes synthesized by CVD. Our results show that the morphology of the flakes and the concentration of Nb interstitials between the NbS_2 layers are highly dependent on the temperature of $NbCl_5$ precursor and the position of the substrate. Samples grown at high $NbCl_5$ temperature or substrate located close to the $NbCl_5$ source show higher incorporation of Nb interstitials. However, the Nb interstitials are not homogenous across the thickness of the sample. High concentration of Nb was detected at the bottom of the flake and reduces with increasing thickness. Electrical measurements carried out show that the samples are indeed metallic with relatively low resistivity.

Conflicts of interest

There are no conflicts to declare

Acknowledgements

This work was supported by the Ministry of Education Malaysia AKU254: HICoE Phase 2 and FRGS/1/2019/STG07/UKM/02/6. MC, JY acknowledge financial support from AFOSR FA9550-16-1-0289. MC, YW acknowledge support from NSF ECCS-1608389. MC acknowledges support from Shenzhen Peacock Plan (Grant No. KQTD2016053112042971). HYJ acknowledges the support from Creative Materials Discovery Program through the National Research Foundation of Korea (NRF-2016M3D1A1900035).

References

1. J. D. Benck, T. R. Hellstern, J. Kibsgaard, P. Chakthranont, and T. F. Jaramillo, *ACS Catalysis*, 2014, **4**, 3957.
2. T. F. Jaramillo, K. P. Jørgensen, J. Bonde, J. H. Nielsen, S. Horch, and I. Chorkendorff, *Science*, 2007, **317**, 100.
3. J. Kibsgaard, Z. Chen, B. N. Reinecke, and T. F. Jaramillo, *Nature Materials*, 2012, **11**, 963.
4. Q. Lu, Y. Yu, Q. Ma, B. Chen, and H. Zhang, *Advanced Materials*, 2016, **28**, 1917.
5. X. Zhang, Z. Lai, C. Tan, and H. Zhang, *Angewandte Chemie International Edition*, 2016, **55**, 8816.
6. C. Tsai, K. Chan, J. K. Nørskov, and F. Abild-Pedersen, *Surface Science*, 2015, **640**, 133.
7. D. Voiry, M. Salehi, R. Silva, T. Fujita, M. Chen, T. Asefa, V. B. Shenoy, G. Eda, and M. Chhowalla, *Nano Letters*, 2013, **13**, 6222.
8. M. A. Lukowski, A. S. Daniel, F. Meng, A. Forticaux, L. Li, and S. Jin, *Journal of the American Chemical Society*, 2013, **135**, 10274.
9. M. Acerce, D. Voiry, and M. Chhowalla, *Nature Nanotechnology*, 2015, **10**, 313.
10. G. Eda, H. Yamaguchi, D. Voiry, T. Fujita, M. Chen, and M. Chhowalla, *Nano Letters*, 2011, **11**, 5111.
11. W. Ge, K. Kawahara, M. Tsuji, and H. Ago, *Nanoscale*, 2013, **5**, 5773.

12. T. Yanase, S. Watanabe, M. Weng, M. Wakeshima, Y. Hinatsu, T. Nagahama, and T. Shimada, *Crystal Growth & Design*, 2016, **16**, 4467.
13. S. Zhao, T. Hotta, T. Koretsune, K. Watanabe, T. Taniguchi, K. Sugawara, T. Takahashi, H. Shinohara, and R. Kitaura, *2D Materials*, 2016, **3**, 025027.
14. X. Wang, J. Lin, Y. Zhu, C. Luo, K. Suenaga, C. Cai, and L. Xie, *Nanoscale*, 2017, **9**, 16607.
15. J. K. Dash, L. Chen, P. H. Dinolfo, T.-M. Lu, and G.-C. Wang, *The Journal of Physical Chemistry C*, 2015, **119**, 19763.
16. Y. Liu, J. Wu, K. P. Hackenberg, J. Zhang, Y. M. Wang, Y. Yang, K. Keyshar, J. Gu, T. Ogitsu, R. Vajtai, J. Lou, P. M. Ajayan, Brandon C. Wood, and B. I. Yakobson, *Nature Energy*, 2017, **2**, 17127.
17. H. Li, H. Wu, S. Yuan, and H. Qian, *Scientific Reports*, 2016, **6**, 21171.
18. D. Hodouin, *Metallurgical Transactions B*, 1975, **6**, 223.
19. J. Huster and H. F. Franzen, *Journal of Less-Common Metals*, 1985, **113**, 119
20. F. Jellinek, G. Brauer, and H. MÜLler, *Nature*, 1960, **185**, 376.
21. F. Kadijk and F. Jellinek, *Journal of the Less Common Metals*, 1969, **19**, 421.
22. Claire J. Carmalt, Emily S. Peters, Ivan P. Parkin, Troy D. Manning, and Andrew L. Hector, *European Journal of Inorganic Chemistry*, 2004, **2004**, 4470.
23. L. S. Price, I. P. Parkin, A. M. E. Hardy, R. J. H. Clark, T. G. Hibbert, and K. C. Molloy, *Chemistry of Materials*, 1999, **11**, 1792.
24. S. Onari, T. Arai, R. Aoki, and S. Nakamura, *Solid State Communications*, 1979, **31**, 577.
25. W. G. McMullan and J. C. Irwin, *Solid State Communications*, 1983, **45**, 557.
26. J. Yang, A. R. Mohmad, Y. Wang, R. Fullon, X. Song, F. Zhao, I. Bozkurt, M. Augustin, E. J. G. Santos, S. H. Shin, W. Zhang, D. Voiry, H. Y. Jeong, and M. Chhowalla, *Nature Materials*, 2019, **18**, 1309.